Katherine Cox

GEOL394

Advisors: Mong-Han Huang, Gimena Chaves Fitzgerald

Assessing the feasibility of NDVI as a tool for slow-moving landslide identification along the Creeping San Andreas Fault

Scientific Abstract

Under predicted climate change effects mass wasting events including slow-moving landslides (SML) are expected to become increasingly common, however the extremely low velocities of these events make them difficult to identify until after slope failure has occurred, placing human lives and infrastructure at risk. Current capabilities in SML identification are limited, and primarily accomplished through InSAR analysis, which is subject to surface feature interference, and fieldwork, which is expensive and logistically difficult in rugged and remote locations, necessitating the development of remote methods to identify these hazards. Understanding porewater availability as a primary positive control on slope failure and vegetation health, the Normalized Differential Vegetation Index (NDVI) can be used as a proxy for slope deformation, so that a feasible relationship between trends in NDVI and SML occurrence may exist. Applying a variational Bayesian Independent Component Analysis (vbICA), a type of independent component analysis that isolates components of a signal providing a framework for the isolation of SML deformation and NDVI components, procedure to current InSAR data of known SMLs and NDVI data, the spatiotemporal effects of both data sets are isolated and compared over the same region and time frame to assess the precise nature of the correlation between the two. Additionally, equal geometry paired SML and stable slope (SS) regions are sampled to test for a significant statistical NDVI difference between the two slope types using statistical distribution and pairwise difference analysis techniques. Results of the study reaffirm the positive hydrologic control of pore water on vegetation health and SML deformation through the emergence of seasonality, but do not display evidence of significant difference in NDVI between the slope types. Results of the NDVI vbICA analysis indicate that IC component 1 is associated with the fault motion of the CSAF while other components are associated with local topography and wet-dry seasons, and time series analysis suggests a possible relationship between NDVI and slope type that warrants further investigation. It is possible that due to the geographical and temporal constraints of this study, there was not sufficient evidence to draw conclusions about the relationship between NDVI and slope stability. However, the methodology utilized by this study provides insight to the complicated nature of SML mechanics highlighting the continued importance of researching methods of SML identifications. This suggests that while NDVI alone is not a valid metric for SML identification, the methodology used shows potential for future analysis.

Plain Language Abstract

SMLs are a variety of landslides characterized by extremely low velocities over long periods of time, making them extremely difficult to detect and monitor. In this, SMLs can exist largely unknown for years so that human infrastructure is often built in the path of these hazards, and millions of dollars in damage is inflicted on this infrastructure every year and placing human life at risk. Current capabilities in identifying SMLs are limited to the monetary and feasibility

constraints of fieldwork, and current remote sensing identification techniques are not entirely comprehensive necessitating the development of expanded ways to use remote sensing to identify these hazards. One primary control on SML failure is porewater availability which reduces the soil strength causing it to fail in a wasting event, with porewater also being a primary control on vegetation health, indicating that the health of the surface vegetation may be indicative of regions prone to SML failure. To assess the possibility of this relationship, a remote sensing technique known as the Normalized Differential Vegetation Index (NDVI) which assessed plant health, is used to proxy soil moisture content alongside deformation data from known SML localities, and on SSs through a combination of signal processing and statistical techniques. Results indicate that there is no significant relationship between NDVI and SML occurrence, so that NDVI alone cannot be used to identify SMLS. However, the methodology shows potential for future analysis.

Introduction & Background

Landslides

In a world becoming increasingly more vulnerable to natural disasters associated with climate change, the slow-moving landslide (SML) is often an overlooked hazard that poses significant risk to human health and safety worldwide. SMLs are a type of geologic hazard categorized as the slow movement of accumulated material downslope under the influence of gravity in a mass wasting event, in a similar fashion to their faster cousins that catastrophic landslides which happen suddenly with little to no warning. These are widely known to wreak devastation on communities, such as in the case of the 2014 Washington State Oso that resulted in 43 deaths and millions of dollars in infrastructure damage (U.S Geological Survey, 2017). SMLs on the other hand are primarily characterized by extremely low velocities falling in the range of 3-5 cm/year and the fastest SML on record, Colorado's Slumgullion Earthflow, only reaches a maximum velocity of 6 m/year (Coe et al., 2003). However, while the low velocities of SMLs mean they pose less direct risk to human life than other landslides, their unique properties create a set of associated hazards that cannot be ignored.

The low velocities of SMLs give them incredible longevity with the oldest known SML being found to be active over 1,000 years ago (Chleborad, A., 2012), categorizing them as long term threats to infrastructure by creating long periods of near perpetual ground deformation. Without knowledge of their localities, humans often build infrastructure in the path of these hazards, resulting in millions of dollars in infrastructure damage. One such case in occurred in Jackson, Wyoming in 2014, where over the course of a few days a SML tore a house in half (Associated Press, 2014).



Figure 1 SML in Jackson, Wyoming tearing house in half (Associated Press, 2014)

SMLs are also still actively failing slopes and have the potential to rapidly transition into catastrophic failure, such as in the case of California's 2017 Mud Creek Landslide (Cueva et al., 2025; Handwerger et al., 2019). As a variety of mass wasting, SMLs possess near identical failure mechanisms to their rapid cousins and see reductions in the internal strength and the accumulation of stress in the soil mass overtime exceeds a minimum shear stress threshold for failure, initiates sliding at depth along a slip plane (Zhang et al., 2011). In the literature, it is found that while there are multiple factors that contribute to failure, such the underlying lithology and slope angle, with the importance of each factor varying between localities, it is agreed that one of the most powerful controls on when this failure occurs is soil pore water availability. Here, higher water levels in the soil are known to reduce internal friction of the slope, weakening it, so that there is a known positive hydrologic control on slope failure. Additionally, the ground infiltration of precipitation through ground cracks is known to raise the local water table, inducing seasonal periodicity in SML motion, similar to health trends seen in vegetation, that aligns with the wet-dry season of their localities (Handwerger et al., 2022). This effect is observed worldwide and is notably present in North America, being seen in Colorado's well-known Slumgullion Earthflow and in California (Handwerger et al., 2013; Coe et al., 2003). This also means that with the increasingly unpredictable extreme weather and major precipitation events associated with climate change, SML occurrence has become harder to predict.

The extremely low velocities of SMLs also makes them incredibly difficult to identify. Without rapid deformation, they do not develop the typical surface deformation features, like the easily identifiable fault scarp of catastrophic landslides, as vegetation has time to grow over the exposed earth. This makes it almost impossible to determine their location from true color aerial photographs leaving field observations, like the curved tree trunk associated with soil creep (Parizek and Woodruff, 1957) and the ground cracks easily misattributed to fault deformation as their only definitive identification method. However, due to the expensive nature of field work as

well as the inaccessibility of the often remote and rugged terrain in which SMLs are prone to, this is not always a feasible option.

Remote Sensing

While ground data is currently the only sure method of determining SML locality, this is not the only method existing for their identification. Numerous remote sensing techniques have already been developed in this area and greatly expand our ability to monitor SMLs. However, despite the massive progress these existing techniques bring, existing remote SML identification techniques are not comprehensive, making it essential to expand capabilities in this field.

Remote sensing describes all techniques of obtaining ground information from a distance, using sensors mounted on satellites or other platforms. There are two types of remote sensing: active remote sensing, which encompasses sensors that send their own electromagnetic pulses towards the ground to determine surface properties in techniques such as InSAR, and passive sensing which relies entirely on the decoding of ground-reflected electromagnetic radiation emitted by the sun, or spectral data (NASA, 2025a). To interpret spectral data in passive remote sensing, satellites like Landsat and Sentinel are equipped with sensors that capture the reflected light radiation coming off the ground in a way taking 'pictures' of the ground pixels. This collected reflected light is categorized by the sensors by the type of light they are, sorting frequencies into bands based on their color of the visible light spectrum, and frequencies in other light categories like infrared and ultraviolet.

The primary remote tool used in SML identification is Interferometric Synthetic Aperture Radar, or InSAR. InSAR is an active remote technique that analyzes changes in ground elevation to identify deforming regions InSAR. This provides highly accurate information to the millimeter scale of ground changes, but while a powerful tool, is not all encompassing. As a reflected radar technique, InSAR data is vulnerable to uncertainty from the addition of noise due to reflectors and other ground cover materials that can scatter the signal, making it less precise like vegetation from tree cover. This necessitates the development of remote sensing techniques that can patch the gap in InSAR capabilities to increase the accuracy of SML monitoring efforts. In this, spectral data is of particular interest for this project, as its usefulness relies on the interpretation of the amounts of and ratios between specific reflected wavelengths to determine ground data. This is done by combining different wavelength data to calculate indices that are specified to reveal different information.

The index of interest for this project is the Normalized Difference Vegetation Index (NDVI), which is a spectral index designed to assess the health of the ground vegetation suggesting it has the potential to bridge the information gap created by InSAR interference. It is calculated as the difference between the total amount of near-infrared (NIR) and red light over the sum of the two for each ground pixel as shown in Equation 1. NDVI can then be described as

the normalized difference between vegetation greenness and density on a scale of -1 to 1. From this, all NDVI values less than zero will correspond to unvegetated regions, and all positive values will correspond to vegetated areas with the health of the vegetation increasing towards 1 (NASA, 2026).

Equation 1:

$$\boldsymbol{NDVI = (NIR - RED)/(NIR + RED)}$$

There are two major satellite programs that collect remote data used in spectral indices, and they are the Landsat and Sentinel programs, managed by the U.S.G.S and the European Space Agency (ESA) respectively. The Landsat program has been active since 1972 with the launch of Landsat-1, and is a satellite ground data program managed by the United States Geological Survey. Currently, it maintains two active satellites - Landsat-8, which was launched in 2013, and more recently Landsat-9 which launched in 2021. Each satellite is equipped with an Operational Land Imager (OLI) capable of processing data in nine spectral bands, and a Thermal Infrared Sensor (TIRS). Landsat-8 is the primary satellite used for spectral data in this project, and processes red light data between 0.64 - 0.67 micrometers in band 4 and NIR light between 0.85 - 0.88 micrometers as band 5. These data are collected with a spatial resolution of 30 m and a temporal resolution of 16 days that is reduced to 8 to 9 days when used in tandem with data from Landsat-9, whose orbit lags behind Landsat-8 and maintains equal resolutions (Landsat Missions, 2025). The Sentinel missions consist of the Sentinel-1 and Sentinel-2 satellites operated by the European Space Agency (ESA), with NASA participating in data distribution and processing to create products such as those offered by the Alaska Satellite Facility (ASF). Sentinel-1 is equipped with a synthetic aperture radar (SAR), while Sentinel-2 is equipped with a Multispectral Imager (MSI) which functions similarly to Landsat's OLI and grants it equivalent capabilities in land usage monitoring. Sentinel-2 processes red and NIR light in bands 4 (0.664 micrometers) and 8 (0.832 micrometers) respectively to a maximum spatial resolution of 10 m, with a temporal resolution of 6 to 12 days (NASA, 2025b). All data used in this study was collected by either the Landsat or Sentinel mission satellites.

Research Premise

Mass wasting is known to be a hydrologically dependent process, with increases in the groundwater table due to rainwater infiltration having substantial control over slope stability due to its capacity to regulate pore water pressure. This process is known to have similar controls on SML deformation velocities (Marte and Ramoser, 2024; Handwerger et al., 2022; Collison and Anderson, 1996; Iverson and Major, 1987) with previous studies confirming SML acceleration

increases in conditions of high pore water pressures (Handwerger et al., 2022). This shows the tendency of SMLs to retain pore water post-infiltration and fail, while nearby stable slopes (SSs) exposed to equivalent amounts of precipitation do not. This is especially in regions with a high concentration of ground cracks which enable infiltration and elevated water tables (Collison and Anderson, 1996), such as active fault zones, are more prone to SML incidence. In fact, one such area in central California along the creeping section of the San Andreas Fault (CSAF) reports over 150 known SMLs, with 60% falling within 1 km of the fault and 75% within 2 km (Scheingross et al., 2013).

Water is essential to plant life. From this, it is reasonable to conclude that regions of elevated groundwater content will also maintain healthier vegetation. In fact, it has been found that wet years correspond with higher NDVI values and therefore healthier vegetation than dry ones (Aguilar et al, 2012). This indicates that the positive relationship between precipitation and vegetation health will overlap with regions prone to SML occurrence, due to a shared positive hydrologic control on vegetation health and slope stability. This relationship allows for the appropriate use of NDVI as a proxy measurement for soil moisture that can be determined from spectral indices alone. In fact, the ability of NDVI to successfully proxy soil moisture content has been documented in the work of Ibañez-Aparicio et al. (2025), which extracted the NDVI from grasslands surrounding an irrigation trench in the Mediterranean mountain area of Spain. Here, the NDVI increased with increasing soil water content. This allows NDVI to be used as a proxy for soil moisture to identify regions susceptible to SML onset through their greater ground water retention.

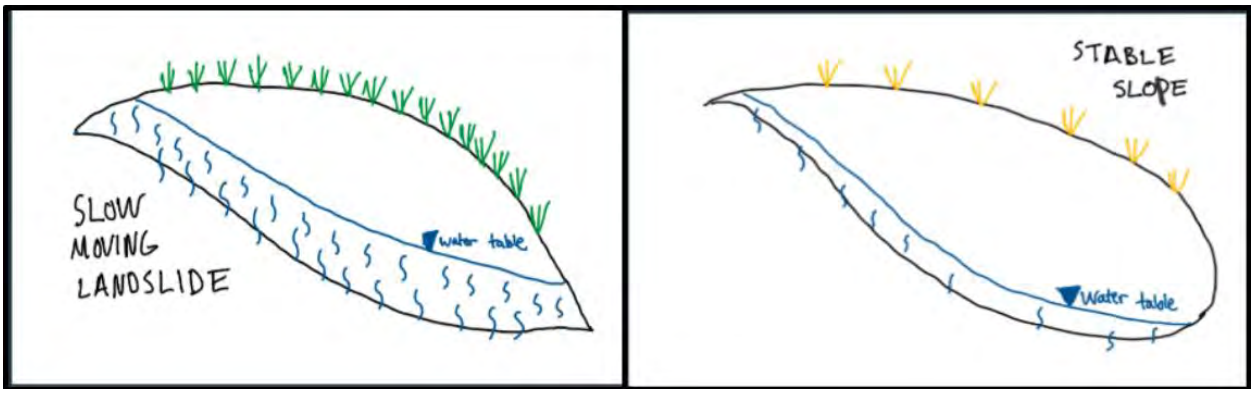


Figure 2 *comparison of hydrologic control on SML and non-SML deformation and NDVI*

Project Objectives and Hypothesis

The goal of this project is to assess the feasibility of using NDVI and spectral data as a means of identification for SMLs. Under the research premise outlined above, the null hypothesis for this study asserts that there will be no relationship between NDVI and SML occurrence, while the alternative hypothesis asserts that there will be an observable trend in NDVI and SML occurrence. If a relationship is found, NDVI will be able to be used as a valid

additional metric for SML identification, improving the capabilities of SML monitoring efforts in vegetated areas. If no relationship between NDVI and slope behavior is found, NDVI cannot be used as a tool to bridge this gap and an investigation into other methods is still necessary.

To test this, NDVI and SML deformation trends along a section of the CSAF were examined. This was done in phases. The first phase aimed to update a repository of known SMLs along the CSAF first categorized by Scheingross et al. (2013), by analyzing horizontal velocity information from NASA ARIA program between January 1, 2018, and August 31, 2021. The second phase consisted of a compared analysis of the calculated NDVI of known SML and non-SML regions in the area of interest (AOI) over the same time frame.

For this a two-pronged approach was used. The first was an independent component analysis (ICA) procedure applied to the NDVI and InSAR values across a focus area known as SmallBox within the AOI. Independent Component Analysis (ICA) is a technique used to recover the unmixed components/signals from the measured data. This can be a wave, deformation, or anything else that is generated by a mixing of those original sources/components (Comon, 1994, as cited in Gualandi and Liu, 2021), so this approach allowed for the examination of NDVI changes in response to SML motion at a very precise level. The second approach consisted of a statistical distribution analysis of randomly selected SML and SS regions via time series analysis and pairwise difference testing. This allowed for the determination of the statistical significance of the difference in NDVI between slope types in the AOI. This allowed for the formation of informed conclusions regarding the NDVI-SML relationship, and what it means in the context of the environment.

Methodology and Design

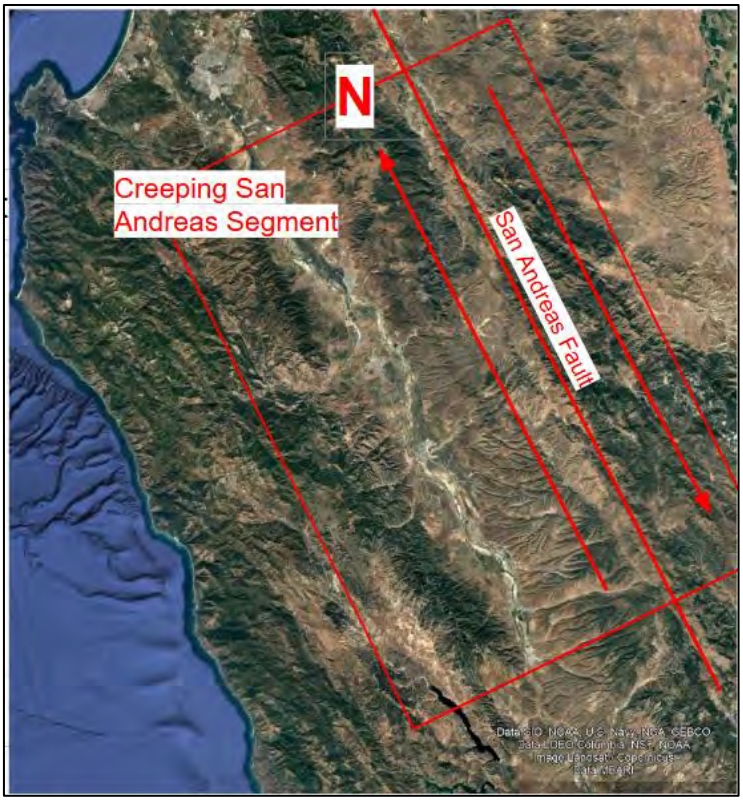


Figure 3 *Shown segment of the CSAF in central California outlined by the red box. North shown by capital N, approximate fault trace shown by solid red line, arrows indicate direction of fault motion.*

Location

To assess this relationship between SML and NDVI, this project focused on analyzing a section of the creeping transect of the CSAF. The San Andreas Fault (SAF) is a major strike-slip fault, where each side of the fault experiences lateral motion relative to the other. It is located in southern to central California and runs approximately North-West to South-East. This region was selected for analysis due to a combination of factors making it an ideal location for this study including a high concentration of known SMLs, a well-documented wet-dry season, and appropriate climate for our analysis.

Success using NDVI as a proxy for soil moisture content was found by Ibanez-Aparicio et al. (2025) in a Mediterranean climate, making it important for this study to focus on a region of a similar climate. This was to maintain as many constants as possible, increasing the reliability of results and success in using NDVI as a groundwater proxy.

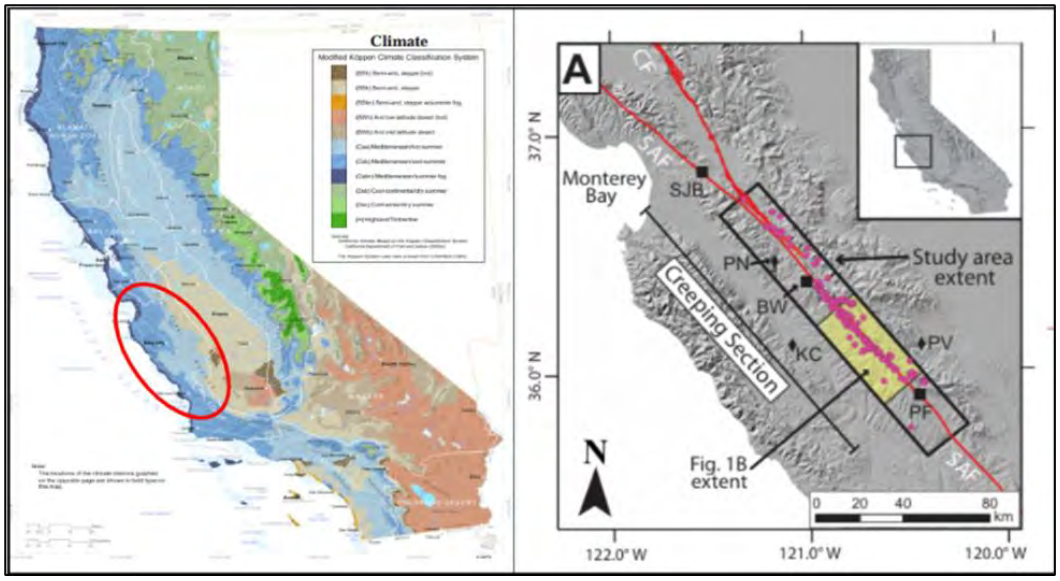


Figure 4 *Side-by-side comparison of a climate map of California and Region of Interests. A) (Left), Circled light blue region indicates AOI overlap with the Mediterranean climate zone (Kaufman, E. Atlas of the Biodiversity of California); b) (Right) , indicated map of AOI with pink dots representing known SMLs (Scheingross et al., 2013).*

As seen in Figure 4a, California experiences a significant region categorized by a Mediterranean climate in the center of the state, as shown by the blue areas. Figure 4b displays a transect of the CSAF with a high concentration of SMLs identified in a repository developed by Scheingross et al (2013) along UAVSAR flightline 14003. A comparison of these two regions reveals that the location of the Scheingross SML repository entirely overlaps with the Mediterranean climate region shown in Figure 4a by the red circle. Therefore, this area with a high concentration of SMLs and an appropriate climate is ideal for the purposes of this experiment and flightline 14003 was designated as the Area of Interest (AOI). However, this area was determined to be too large for appropriate analysis to be conducted over the entirely, so a small region designated as SmallBox was selected as a focus point for analysis due to its combined high density of SMLs, and high resolution NDVI and InSAR data from 2018-2021. The AOI and SmallBox are displayed in Figure. 3.

It is also important to note that the AOI is located along the fracture zone of the SAF, where there is a high propensity of ground cracks resulting from fault motion within 5km of the trace. From this, it was determined that sufficiently large amounts of groundwater infiltrated in this region for SML incidence to occur (Collison and Anderson, 1996; Scheingross et al., 2013). Additionally, while the SAF is known to produce large earthquakes that can induce slope failure, the AOI is located along the creeping segment. Here regional seismicity is characterized by frequent low magnitude earthquakes that are insufficiently large to incite sliding (Scheingross et al., 2013). While this constant activity does contribute to the instability of the slopes in the area and may make them more prone to failure, this assertion means it is reasonably certain that any landslide deformation observed in the AOI is primarily the result of hydrologic rather than seismic controls. Another reason this area was chosen was that California has an extremely well documented wet and dry cycle. This makes it easy to determine seasonal periodicity in the data, so that trends in NDVI and ground deformation can be identified.

Data Preparation

Once the locality for this project was selected, the process of processing the data could begin. The first step in this was to update the Scheingross et al. (2013) repository to reflect current deformation in the area. This was done by downloading open-source InSAR products from the NASA ARIA program. This provided high resolution information about the ground deformation in the area. Utilizing Google Earth Engine (GEE) and QGIS, these data were compared with a modern satellite basemap and regions identified as SMLS in the Scheingross et al. (2013) repository were cross-referenced with current ARIA data to reflect current day SML behavior. The horizontal velocities, or the E-W component, of the ARIA data were used for this, both because the Scheingross repository found SMLs to primarily occur normal to the NW-SE orientation of the SAF shown in Figure 2, and because the orientation of the camera and the polar orbit of the InSAR satellites optimizes their data to determine E-W velocities. This is

another weak point of InSAR based SML identification that NDVI will help cover if a legitimate relationship between deforming slopes and vegetation health is found.

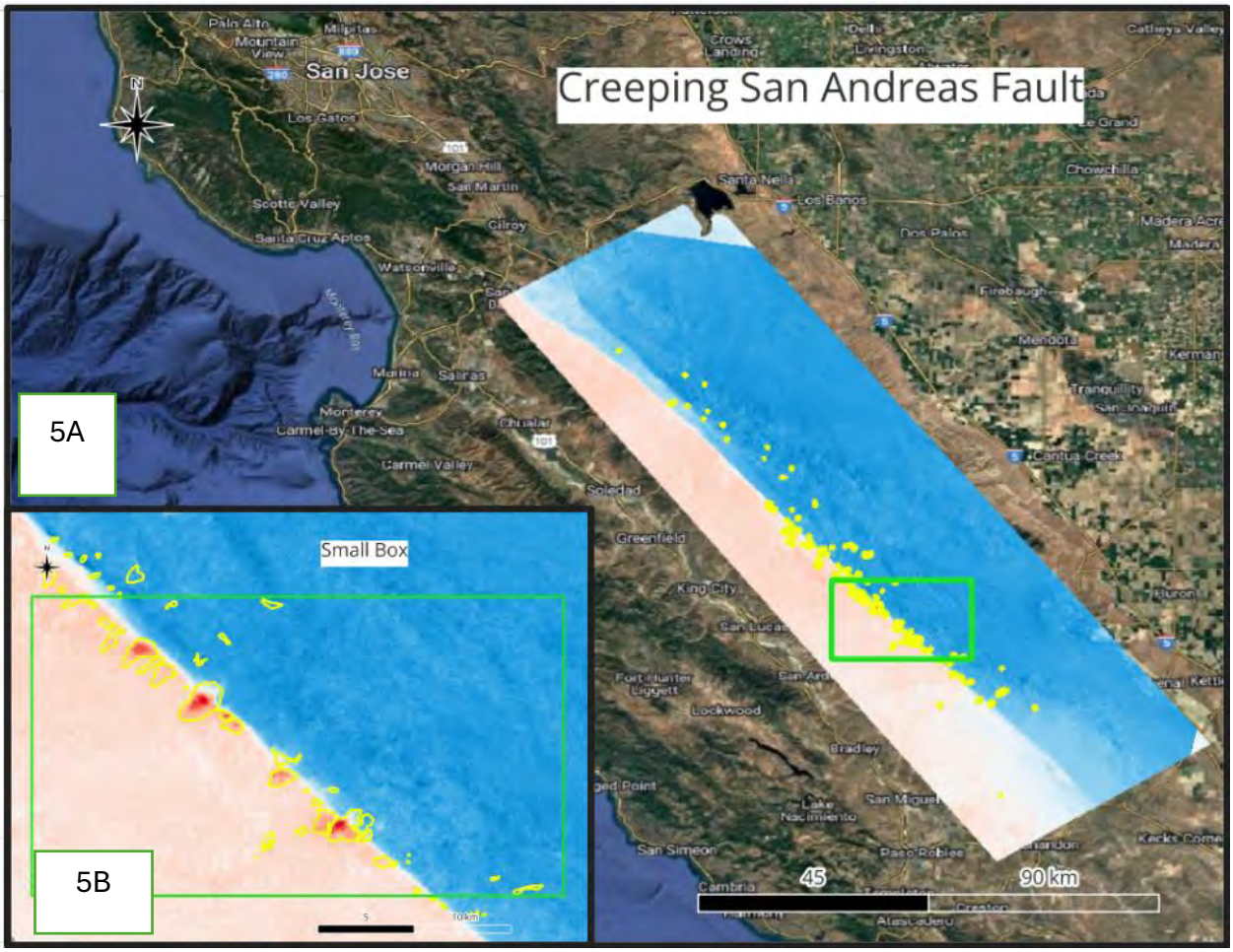


Figure 5 *A) ARIA horizontal velocity map of UAVSAR flightline 14003 along flightline overlaid with known SMLs (yellow) and SmallBox focus region (green). B) SmallBox focus region with horizontal ARIA velocities overlaid by updated SML repository*

Once the SML repository was updated, a GEE script was used to calculate the NDVI of the AOI between 01-01-2018 and 08-31-2018. As spectral data relies on the reflected light from the surface, cloudy pixels block the signals from the ground from reaching the satellite resulting in information degradation. This means that an image with a lot of cloud cover will not be useful, and a threshold for an acceptable amount of cloud cover in the images used must be set. For this experiment, this threshold was set to 10% meaning that no more than 10% of the image could contain clouds.

From these remaining images, the two best pictures within the SmallBox focus area were selected and downloaded for each month, creating an NDVI log. These images were then filtered to share a common pixel for ease of comparison.

Methodology

To analyze the collected NDVI data for the AOI and SmallBox, a two-method approach was used. The first method consisted of an ICA method designed to assess the interplay of NDVI with InSAR ground velocity between SML and non-SML slopes. The second, was a pairwise distribution analysis of the NDVI time series between SML and SSs, allowing for the determination of a statistically significant difference in NDVI between the slope types. The combination of these techniques allowed for the development of a comprehensive picture of the region and in-depth evaluation of the potential relationship between SML and NDVI.

Independent Component Analysis (ICA)

The ICA procedure for this experiment was a Variational Bayesian Independent Component Analysis (vbICA) algorithm, derived from the work of Gaulandi and Liu (2021) which optimized both InSAR analysis and provided a framework for the decomposition of NDVI signals. As this algorithm was developed using data from a region in California overlapping with the AOI, and ICA procedures have been found to successfully decompose and interpret NDVI signals in the past as related to hydrologic events (Antico, 2011), this method was perfect for the purposes of this experiment. Hence, running the SmallBox NDVI data through the Gualandi and Liu (2021) vbICA procedure, decomposed the signal successfully into 6 individual components that could be interpreted through the lens of hydrologic changes in the area. By feeding the InSAR data for SmallBox over the same time frame through this same procedure, the deformation signal was broken down into four components. From the SML overlay of the individual components, it was determined the component 1 (InSAR IC 1) corresponded to SML deformation. InSAR IC 1 was then used to isolate SML deformation from CSAF fault creep, to accurately compare the NDVI components for SML and SS regions and identify associations in NDVI and slope deformation.

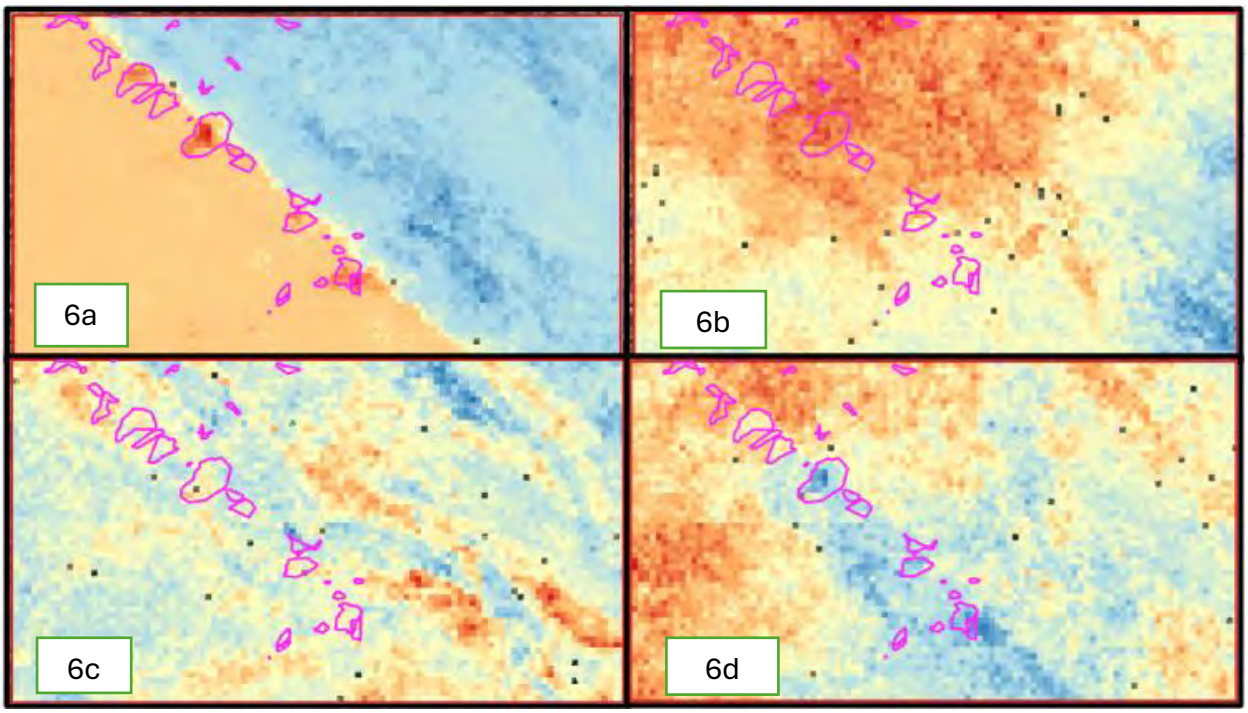


Figure 6 *A) InSAR ICA component 1 B) InSAR ICA component 2 C) InSAR ICA component 3 D) InSAR ICA component 4*

Statistical Distribution Analysis

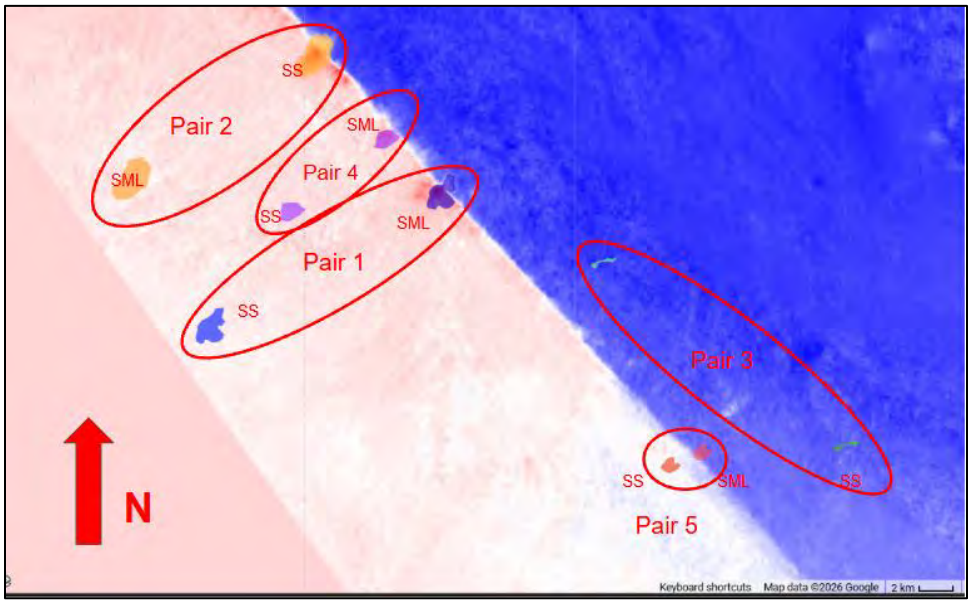


Figure 7 Map of the 5 SML-SS pairs

For the statistical distribution analysis, five SML - SS pairs were created to conduct pairwise NDVI analysis across the AOI. Each pair was created by randomly selecting an active SML from the updated SML repository and copying the geometry to a stable region to form the paired SS. Using these pairs, time series, density distribution, and pairwise difference analysis of t-test and Wilcoxon tests were performed. Wilcoxon tests are suitable for non-parametric data (Kim, 2014).

Data

NDVI ICA Procedure

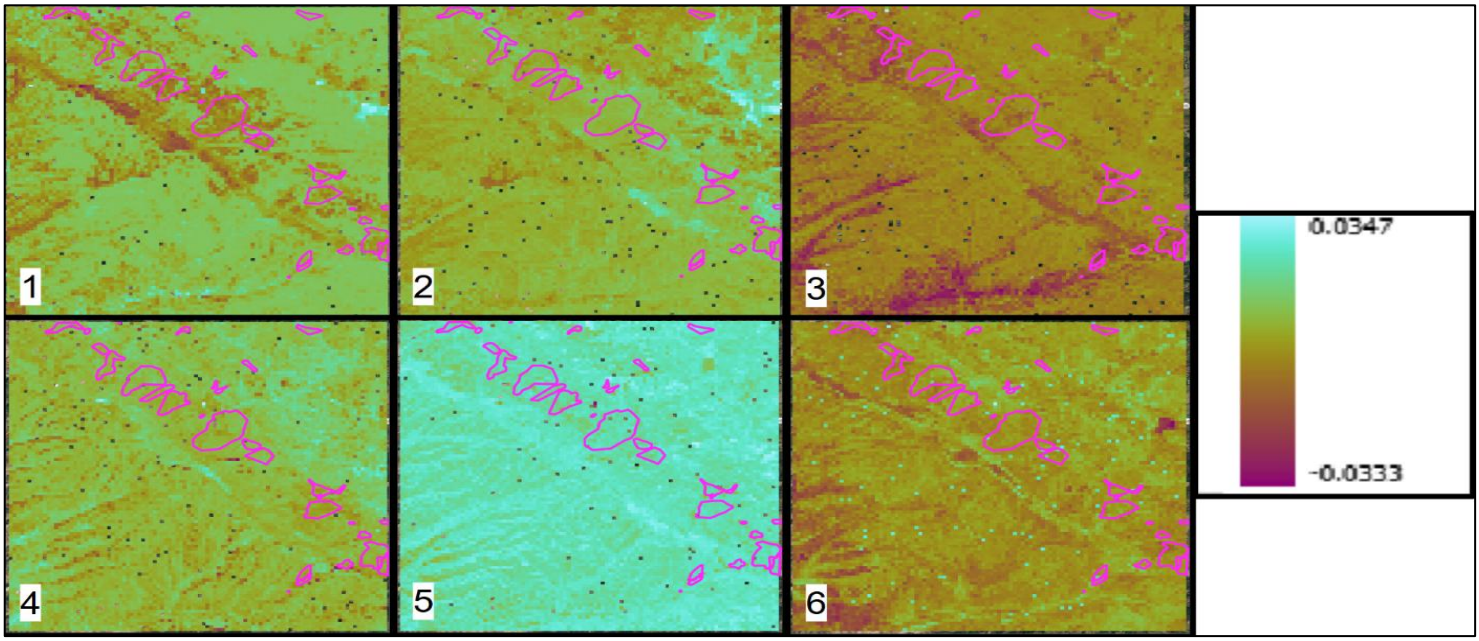


Figure 9 *SmallBox NDVI vbICA components 1-6 for 01-01-2018 to 08-31-2021 in order from top left to bottom right*

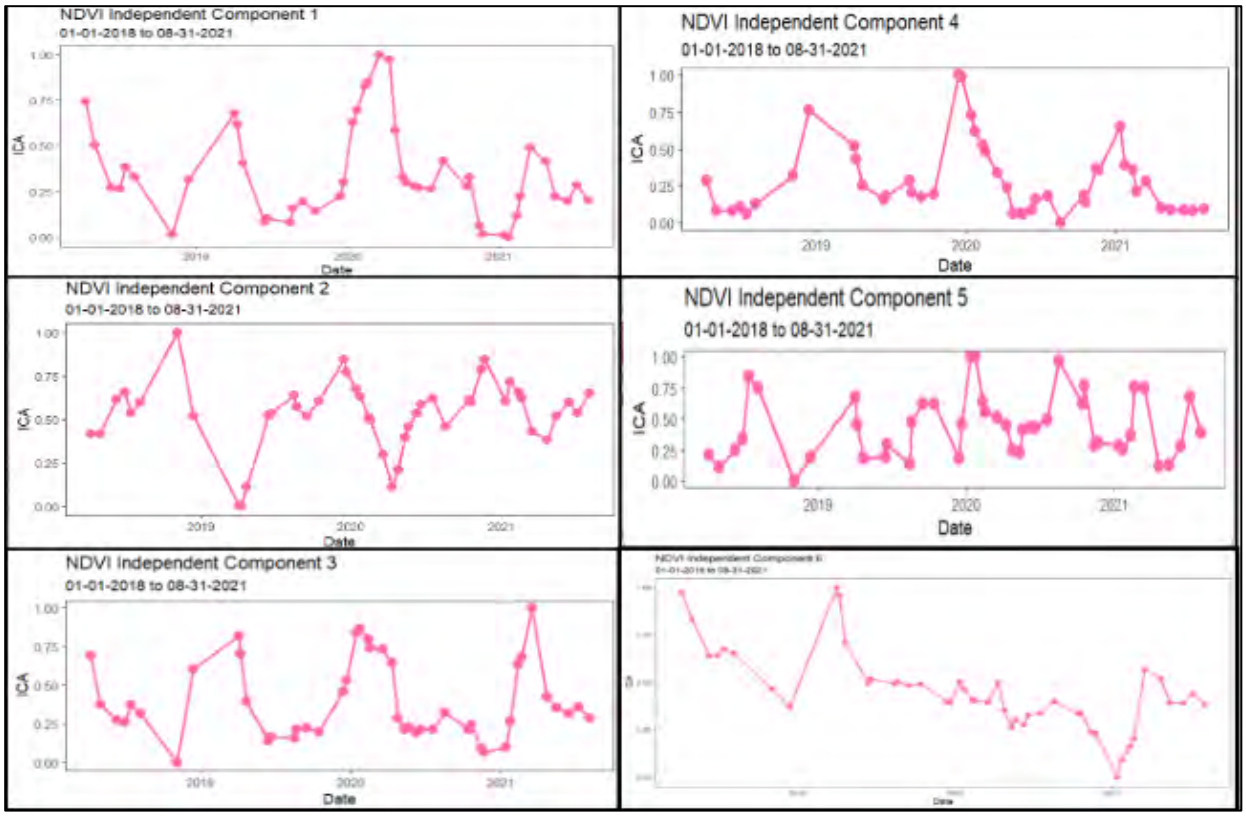


Figure 8. *Time series distribution of NDVI IC components 1-6*

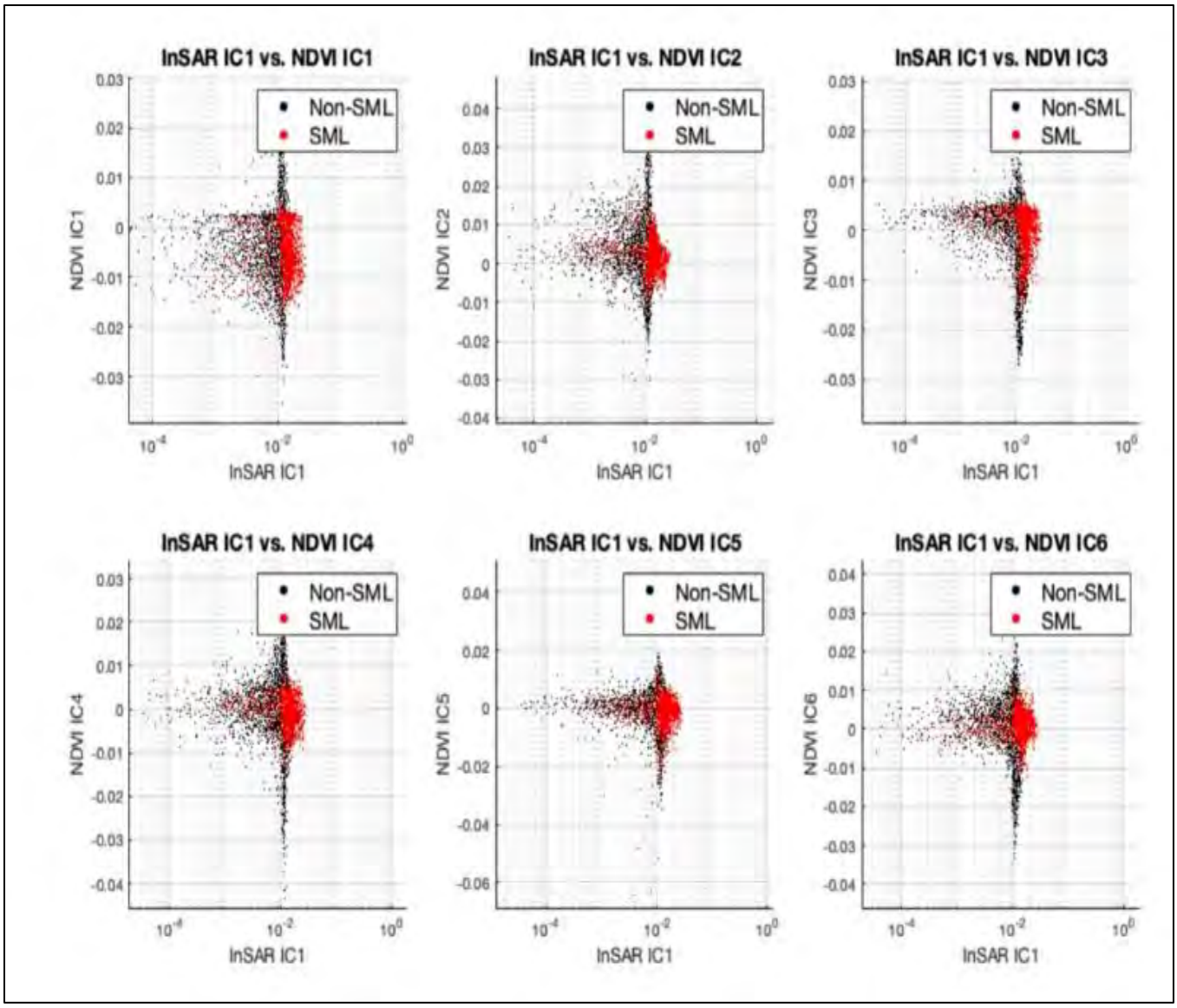


Figure 10 *From top left to bottom right interpolated InSAR IC 1 and NDVI IC 1 plots for SML and Non-SML regions in the AOI.*

Paired SML-SS Distribution Analysis

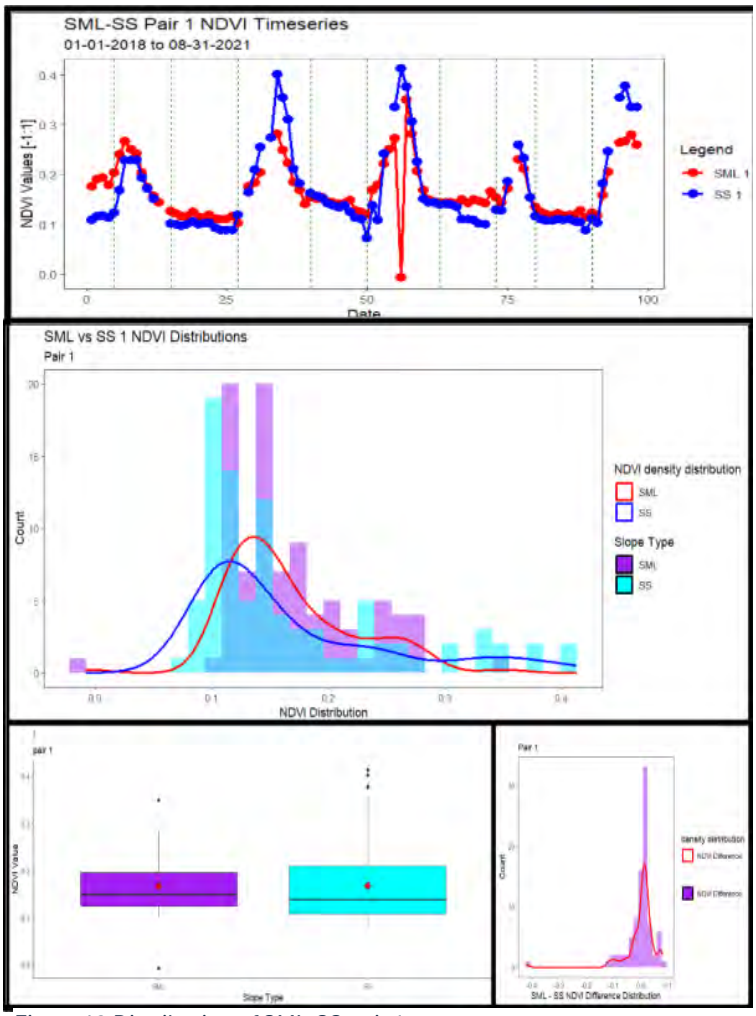


Figure 12 Distribution of SML-SS pair 1

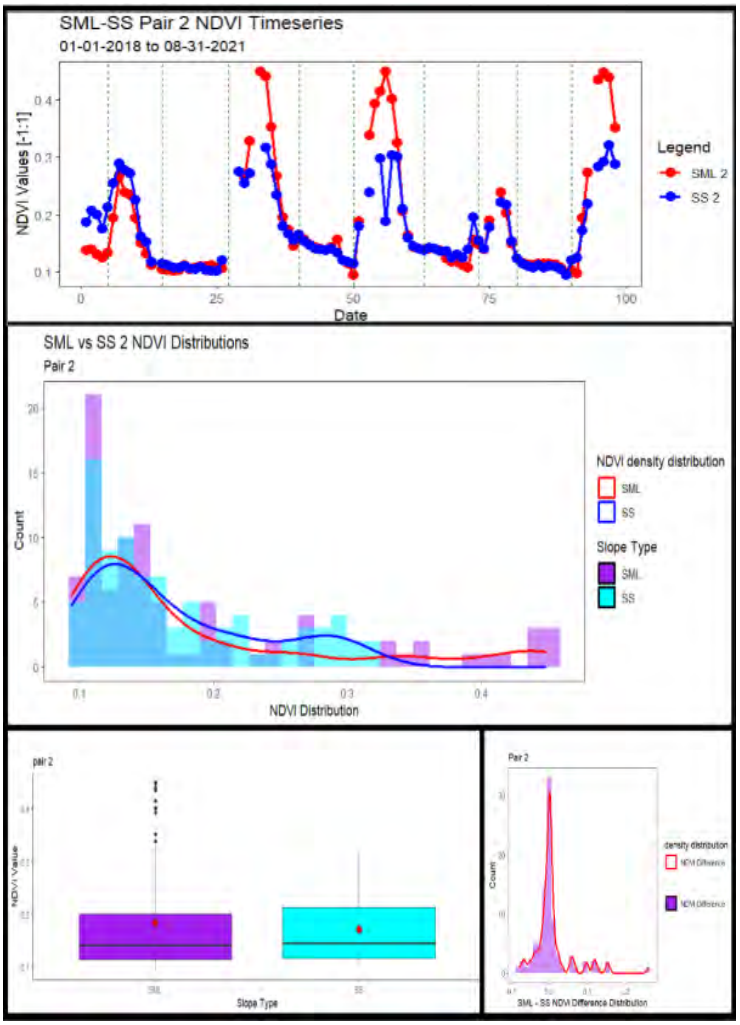


Figure 11 Distribution of SML-SS pair 2

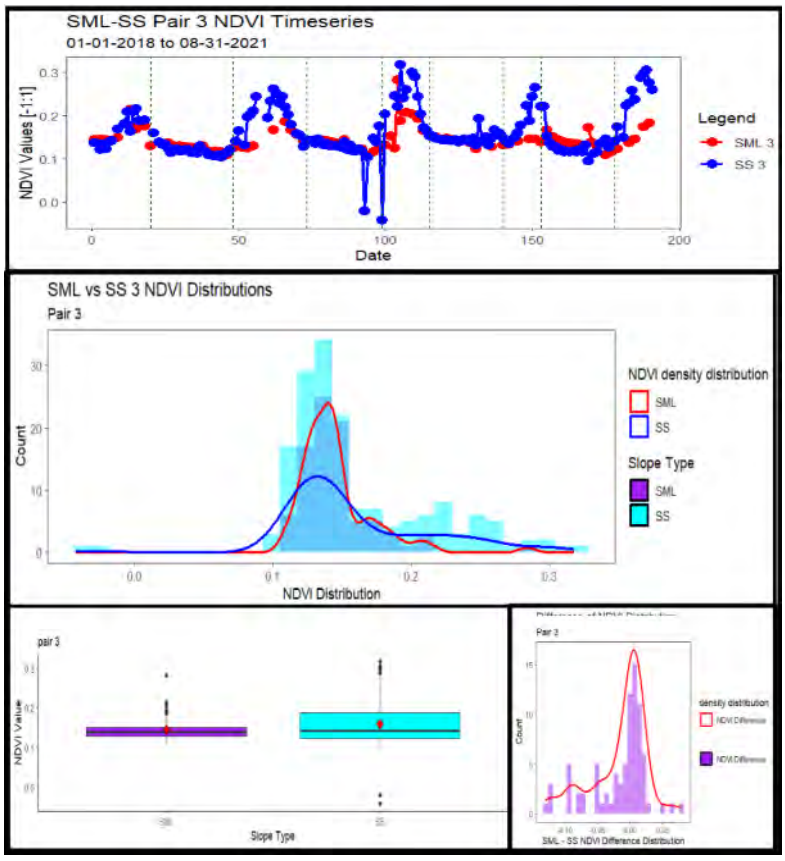


Figure 13 Distribution of SML-SS pair 3

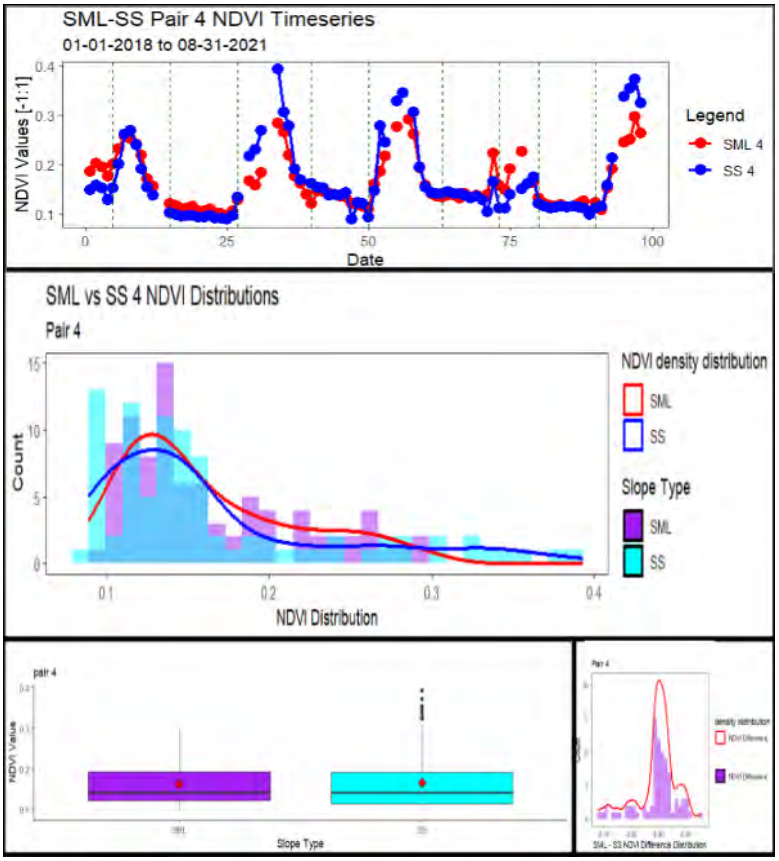


Figure 14 Distribution of SML-SS pair 4

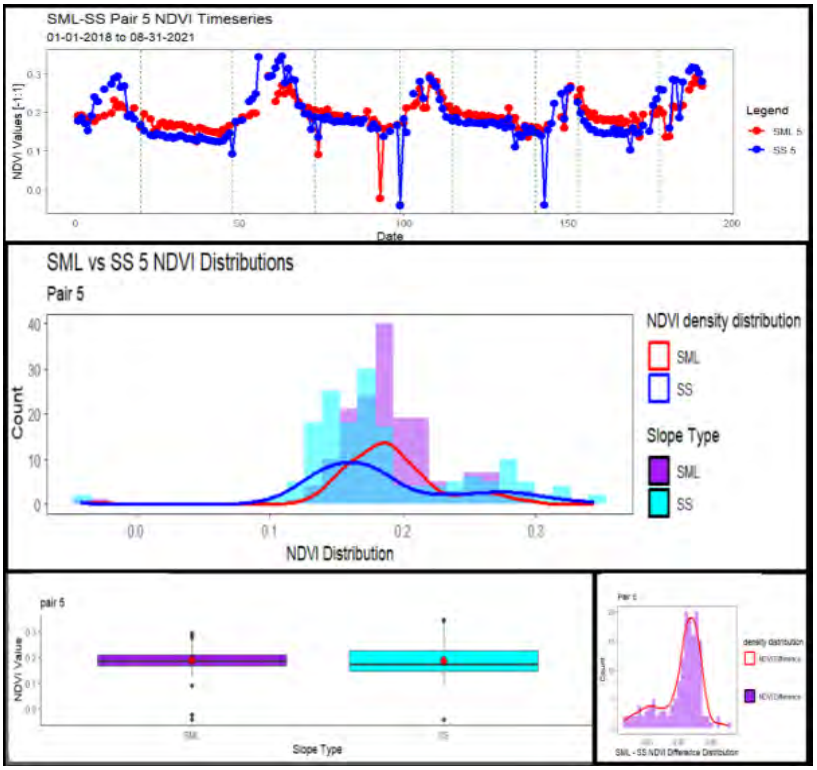


Figure 15 Distribution of SML-SS pair 5

Table 1: SML and non-SML mean and paired t-test distribution analysis

Paired t-test (α=0.05)												
	Pair 1		Pair 2		Pair 3		Pair 4		Pair 5		Total	
	SML	SS	SML	SS	SML	SS	SML	SS	SML	SS	SML	SS
Mean	0.166	0.167	0.183	0.171	0.145	0.160	0.163	0.166	0.190	0.187	0.170	0.170
CI	[-0.023, 0.0199]		[-0.012, 0.039]		[-0.024, -0.004]		[-0.023, 0.016]		[-0.009, 0.013]		[-0.023, 0.214]	
t-value	-0.122		1.030		-2.790		-0.368		0.427		-0.077	
p-score	0.903		0.305		0.006		0.713		0.670		0.9406	

Table 2: SML and non-SML median and paired Wilcoxon test distribution analysis

Wilcoxon Test										
	Pair 1		Pair 2		Pair 3		Pair 4		Pair 5	
Median	SML	SS	SML	SS	SML	SS	SML	SS	SML	SS
	0.149	0.138	0.141	0.145	0.140	0.142	0.142	0.142	0.187	0.174
V	2369.5		1957		1362.5		1966		8364.5	
P-value	0.05413		0.7111		0.1176		0.5454		0.005344	

Analysis

In interpreting the results of this study, the most important thing to do is characterize the NDVI vbICA components. Examining Figure 8, which shows each of the six components from left to right starting in the top, an observable overlap between the SMLs (shown in pink) is apparent in component 1. With the understanding that NDVI components can correlate directly to hydrologic effects, the seen alignment of a dark orange-reddish line in a light green region suggests that the SMLs co-occur with areas of lower NDVI than the surrounding regions during specific hydrologic events in the 2018–2021 frame. Examining the other components, it is seen that the remaining 5 components do not appear to have any obvious relationship with SML occurrence. However, it is interesting to note that lower NDVI values in each component indicate drier regions represented by red coloring, and wetter regions with higher NDVIs are represented by teal coloring. Considering this, and the tendency of NDVI ICA components to

associate with hydrologic events, the trends observed in component 1 are most likely to be associated with soil deformation related to SML motion and fault creep as seen in the reddish region aligned roughly along the orientation of the San Andreas Fault. Component 5, being almost entirely teal, is likely associated with a major precipitation event during 2018-2021, while component 3 being almost entirely orange is likely associated with a major dry period. This suggests that Component 5 is representative of NDVI across SmallBox during the wet season and Component 3 is representative of NDVI during the dry season. Component 4 appears to be associated with the topography of the area with drier regions occurring in elevated regions, and wetter ones associated with valleys that are conducive to streams. Component 6 also appears to be associated with topography, with topographic highs reading elevated NDVI compared to the lower areas. From the wetter regions in the northeast corner of component 2, it is most likely associated with a localized hydrologic change in the time frame. This apparent correspondence of the NDVI ICA components to hydrologic events is supported by the underlying theory of this system, and by the observation of cyclicity in the NDVI ICA time series shown in Figure 9.

In observation of the interpolated InSAR IC 1 vs NDVI IC component plots seen in Figure 10, it is notable that the distribution does not appear to change significantly between NDVI IC components despite their correspondence to difference factors. However, this is not to say there is not a trend. Across all 6 IC components, the SMLs shown in red display a significantly narrower range of NDVI than the non-SML regions. It is also interesting to note that the distribution of each NDVI component appears to be centered around zero.

Continuing to the statistical distribution analysis we begin to see more obvious differences between the SML and SS NDVI. In the Pair 1 analysis shown in Figure 11, there is a distinct separation of the SS and SML NDVI distribution peaks in the histogram. Here the SML peak is observed to occur at a higher NDVI value than the SS. This is consistent with the theory the SMLs should maintain higher NDVI values over time than non-SML regions and is also observed in the time series. Here, while the two slope types track approximately on top of each other during the wet season, in the dry season they seem to separate with the SML registering higher NDVI values. However, while this suggests that the is a separation of NDVI between the slope types in pair 1, the overlap of the boxplots indicates this may not be significant. This trend is consistent with the observations made in Figure 12 examining pair 2.

Here, the histogram displays a consistency in NDVI distribution between the SML and SS slopes, which is also seen represented in the time series and near identical box plots. However, in the instances where SML and SS do differ across this pair it is notable that this occurs only where the SML is registering higher NDVI values than the SS. Interestingly, this appears to be during the wet season rather than the dry season as displayed in Figure 11. Figure 13 continues this trend of consistency between the SML and SS slopes, with a notable difference being that in this instance the SS tends to register higher NDVI than the SML. A similar trend is shown for pair 4 in Figure 14. Interestingly, reading Figure 15 showing pair 5 is more similar to pair 1 than any of the other pairs. It too displaces a clear separation of the SML and SS NDVI

distribution with the SML peaking at higher NDVIs than the SS, and the SML registering consistently higher NDVIs in the dry season of the time series than the SS. Despite this, the results of the paired t-tests shown in Table-1 all display p-values greater than 0.05, which when considering the visible separation of the distributions and skew in the histograms suggests that this data is not Gaussian and is better represented by a non-parametric test.

In Table-2 the results of the Wilcoxon non-parametric test for the difference in distributions is shown. Here, it is notable that while Pairs 2, 3, and 4 do not maintain a significant separation of their SML and SS distributions, Pair 1 maintains a Wilcoxon p-value of 0.05413 which is only 0.00413 greater than 0.05 and could be considered 0.413% away from significance. This does not suggest that the difference in SML and SS NDVI distributions of pair 1 is significant because it is not, but it is interesting to note that it comes close to significance while being one of two pairs to display any sort of visible distribution separation. On the other hand, with a Wilcoxon p-value of $0.005233 < 0.05$, the difference between the SML and the SS in pair 5 is significant.

Discussion

Considering the results of the NDVI time series and the vbICA components together, an interesting picture is drawn for the CSAF. While there is evidence of clear seasonality in NDVI trends on both the stable and actively deforming slopes, the extent to which this deformation occurs and whether or not it can be accurately predicted by NDVI is not conclusive. While vbICA component 1 suggests that NDVI on SMLs is lower than the NDVI of SSs, the time series shown in Figure 8 suggests that this phenomenon may only be representative of the wet season as SMLs appear to be retaining higher water levels during the dry season. Additionally, the results of the NDVI vbICA are highly seasonal and sensitive to extreme weather events, with components 3 and 5 appearing to be representative of the dry and wet seasons respectively, and components 4 and 6 appearing to correspond to the seasonal effects of topography.

It is also important to note that the drier regions shown in component 1 are not contained precisely within the SML areas and just have a high rate of overlap with them. There are SMLs shown that do not overlap with these drier regions at all in the northernmost and southern-most regions of SmallBox. It is also interesting to note that the regions of SML overlap with low NDVI also do not correspond to the areas of the lowest NDVI on the map. This is reserved for the region tracing the orientation of the San Andreas Fault. Considering this, it can be reasoned that component 1 may very well correspond with SML deformation, it is more likely to correspond to the overall deformation of the region, including that related to the fracture zone of the SAF. This is especially true considering that the input NDVI data has no spatial component, so the deformation occurring in the region will make itself known in other ways. Additionally, SMLs are found in their highest concentrations in this region near the fault trace (Scheingross, 2013), so it is reasonable to conclude that the N-S deformation of the fault will influence the vegetation health of the region. This is supported by there being no true difference between

NDVI components in the InSAR vs NDVI plots of Figure 10. However considering that the vbICA increases in accuracy with the amount of data it is fed and the relatively small proportion of active SML pixels to total pixels in SmallBox, it is likely that there was not enough data present for the algorithm to distinguish between the comparatively small E-W landslide deformation to the all encompassing N-S deformation of the CSAF. This suggests that if this procedure was to be repeated over a larger area and/or time scale, it is likely to yield more conclusive results.

The statistical distribution analysis of the other hand tells a slightly different story. While there is not enough evidence in this analysis to claim a widespread significant difference in the NDVI distribution of the SMLs and SS across the AOI, the existence of a distinct visible pattern of distribution separation and the significantly higher distribution of the SML NDVI pair 5 under the Wilcoxon test (Figure 15) is consistent with the idea that SMLs will retain more pore water, particularly in the dry season. This suggests that the NDVI distributions of SML and non-SML regions can be expected to be non-Gaussian and that if a similar procedure was applied to a larger sample size a clear pattern of behavior may emerge. However, while these results suggest directions for future work, at the current level of analysis there does not appear to be any significant overarching patterns of behavior between NDVI and SMLs.

Conclusions

From this study of the NDVI and SML behavior along the CSAF this is a complex system, with many variables that interplay with each other to varying degrees between location and in time. It can be concluded that there is a distinct seasonality in the NDVI of SMLs and SSs across the AOI, some evidence suggesting NDVI is elevated on SMLs and some suggesting it is lower on SMLs. This means that with the current level of analysis there is no evidence of a significant relationship between NDVI and SML occurrence along the CSAF, and that NDVI cannot be used alone as a reliable tool to identify SMLs. However, while NDVI has not been found to be a useful metric for landslide identification in this situation, the information gap presented by the limits of field work and InSAR analysis still stands true, necessitating the development of more remote methods to improve SML identification. While NDVI did not prove useful in this instance, a tremendous amount of insight into the complicated mechanisms behind SML deformation was provided by this study, largely yielded from vbICA analysis of spectral and InSAR data. From this, it can be concluded that while NDVI is not a valid metric for SML identification on its own, the methodology by which this was determined shows significant potential for future analysis.

Acknowledgements

I would like to formally acknowledge Dr. Mong-Han Huang, Gimena Chaves Fitzgerald, Dr. Philip Piccoli, and Dr. Mike Evans for their assistance and advice to me in the completion of this project. I would also like to thank my roommates Michelle Reynoso, Pearl Uva, and Lila Wilson for listening to my endless rambles through this project, all their feedback, and for helping me stay outside my head. I could not have asked for better friends. I would also like to thank the Active Tectonics Labs for all their feedback and support of me in doing this project. I could not have done this without any of you. Thank you.

Bibliography

Aguilar, C., Zinnert, C. J., Polo, J. M., Young, R. D. (2012). NDVI as an indicator for changes in water availability to woody vegetation. *Ecological Indicators (23)*, 290-300. https://doi.org/10.1016/j.ecolind.2012.04.008.

Antico, A. (2012). Independent component analysis of MODIS-NDVI data in a large South American wetland. *Remote Sensing Letters, 3:5, 383-392.* DOI: 10.1080/01431161.2011.603376.

Associated Press. (2014). Slow-moving landslide speeds up, splits Wyoming home in two. *NBC news: Politics. https://www.nbcnews.com/news/us-news/slow-moving-landslide-speeds-splits-wyoming-home-two-n84731* .

Chleborad, A. (2012). Radiocarbon age of a newly identified Slumgullion Landslide deposit. *U.S. Geological Survey Bulletin 2130: Chapter 5. http://pubsdata.usgs.gov/pubs/bul/b2130/Chapter5.html.*

Coe, J. A, Ellise, W. L, Godt, J. W., Savage, W. Z., Savage, J. E., Michael, J. A., Kibler, J. D., Powers, P. S., Lidke, D. J., Debray, S. (2003). Seasonal movement of the Slumgullion landslide determined from global position system surveys and field instrumentation, July 1998-March 2002. *Engineering Geology 86* (1-2), 67-101. https://doi.org/10.1016/S0013-7952(02)00199-0.

Collison, A. J., Anderson, M. G (1996). Using a combined slope hydrology/stability model to identify suitable conditions for landslide prevention by vegetation in the humid tropics. *Earth Surface Processes and Landforms 21*(8), 737-747. https://doi.org/10.1002/(SICI)1096-9837(199608)21:8%3C737::AID-ESP674%3E3.0.CO;2-F.

Cueva, M., Kang, X., Wang, S., Soranzo, E., Wu, W. (2025). Unveiling the role of saturation and displacement rate in the transition from slow movement to catastrophic failure in landslides. *Engineering Geology 352*. https://doi.org/10.1016/j.enggeo.2025.108042.

Gualandi, A., Liu, Z. (2021). Variation bayesian independent component analysis for InSAR displacement time-series with application to Central California, USA. *Journal of Geophysical Research: Solid Earth (126)4.* DOI: https://doi.org/10.1029/2020JB020845

Handwerger, A. L., Fielding, E. J., Sangha, S. S., Bekaert, D. P. S. (2022). Landslide sensitivity and response to precipitation changes in wet and dry climates. *Geophysical Research Letters* 49(13). https://doi. org/10.1029/2022GL099499.

Handwerger, A.L., Huang, MH., Fielding, E.J. et al.(2019). A shift from drought to extreme rainfall drives a stable landslide to catastrophic failure. Sci Rep 9, 1569. https://doi.org/10.1038/s41598-018-38300-0

Handwerger, A. L., Roering, J. J., Schmidt, D. A., (2013). Controls on the seasonal deformation of slow-moving landslides. *Earth and Planetary Science Letters 377-378*, 239-247. https://doi.org/10.1016/j.epsl.2013.06.047.

Ibañez-Aparicio, J., Pimentel, R., Bonet-Garcia, J. F., Polo J. M. (2025). Using NDVI-derived vegetation vigour as a proxy for soil water content in Mediterranean-mountain traditional water management systems: Seasonal variability and restoration impacts. *Ecological Indicators 174*. https://doi.org/10.1016/j.ecolind.2025.113468.

Kim, H. (2014). Statistical notes for clinical researchers: Nonparametric statistical method: 1. Nonparametric methods for comparing two groups. *National Library of Medicine: National Center for Biotechnology Information, 39(3), 235-239.* DOI: https://doi.org/10.5395/rde.2014.39.3.235

Landsat Missions (2025). Landsat 8. USGS. Accessed November 12, 2025, from https://www.usgs.gov/landsat-missions/landsat-8.

Marte, R., Ramoser, H. (2024). Prediction program for slow moving landslides. *Geotechnical Engineering Challenges.* DOI 10.1201/9781003431749-219.

NASA (2026). Normalized difference vegetation index (NDVI). EARTHDATA. Retrieved April 27, 2026, from https://www.earthdata.nasa.gov/topics/land-surface/normalized-difference-vegetation-index-ndvi.

NASA (2025a). Remote sensing. NASA EARTHDATA. Retrieved November 28, 2025, from https://www.earthdata.nasa.gov/learn/earth-observation-data-basics/remote-sensing.

NASA (2025b). Sentinel-2 MSI. EARTHDATA. Retrieved November 28, 2025, from https://www.earthdata.nasa.gov/data/instruments/sentinel-2-msi.

Parizek, E. J., Woodruff, J. F. (1957). Mass wasting and the deformation of trees. *American Journal of Science 255*(1), 63-70. https://doi.org/10.2475/ajs.255.1.63.

R., M. Iverson, J, J. Major. (1987). Rainfall, ground-water flow, and seasonal movement at Minor Creek landslide, northwestern California: Physical interpretation of empirical relations. *GSA Bulletin 99*(4), 579–594. doi: https://doi.org/10.1130/0016-7606(1987)99<579:RGFASM>2.0.CO;2.

Scheingross, J. S., Minchew, M. B., Mackey, H. B., Simons, M., Lamb, P. M., Hensley, S. (2013). Fault-zone controls on the spatial distribution of slow-moving landslides. *GSA Bulletin 125*(3-4), 473-489. doi: 10.1130/B30719.1.

United States Geological Survey. (2017). Revisiting the Oso landslide. *United States Geological Survey.* Accessed December 1, 2025, from https://www.usgs.gov/news/featured-story/revisiting-oso-landslide.

Zhang L, L., Zhang J., Zhang L, M., Tang, W, H. (2011). Stability analysis of rainfall-induced slope failure: a review. *Proceedings of the Institution of Civil Engineers - Geotechnical Engineering 164*(5), 299–316. doi: https://doi.org/10.1680/geng.2011.164.5.299.